Understanding the recent increase in multiyear La Niñas

Check for updates

Bin Wang [1] ✉, Weiyi Sun [2,3] ✉, Chunhan Jin [4], Xiao Luo [1,5], Young-Min Yang [6], Tim Li [1], Baoqiang Xiang [7,8], Michael J. McPhaden [9], Mark A. Cane [10], Feifei Jin [1], Fei Liu [11] & Jian Liu [2]

Five out of six La Niña events since 1998 have lasted two to three years. Why so many long-lasting multiyear La Niña events have emerged recently and whether they will become more common remains unknown. Here we show that ten multiyear La Niña events over the past century had an accelerated trend, with eight of these occurring after 1970. The two types of multiyear La Niña events over this time period followed either a super El Niño or a central Pacific El Niño. We find that multiyear La Niña events differ from single-year La Niñas by a prominent onset rate, which is rooted in the western Pacific warming-enhanced zonal advective feedback for the central Pacific multiyear La Niña events type and thermocline feedback for the super El Niño multiyear La Niña events type. The results from large ensemble climate simulations support the observed multiyear La Niña events–western Pacific warming link. More multiyear La Niña events will exacerbate adverse socioeconomic impacts if the western Pacific continues to warm relative to the central Pacific.

Since the start of the twenty-first century, there have been five multiyear La Niña events, including 1998–2000, 2007–2008, 2010–2011, 2016–2017 and 2020–2022 (Fig. 1a). As only 10 multiyear La Niñas have occurred over the past 100 years, the clustered events in the last 25 years are notable. Although progress has been made in El Niño/Southern Oscillation (ENSO) studies during the past few decades, why double and triple La Niña events have become prominent in recent times remains a puzzle.

Understanding the response of multiyear La Niñas to changing climate is essential for mitigating severe natural hazards and protecting socioeconomic systems. Multiyear La Niña events, coupled with global warming and land surface feedbacks, may explain the recent megadrought in North America[1,2]. Thousands of deaths and dramatic economic losses have occurred worldwide during extreme multiyear La Niña weather-related hazards, including severe droughts, heatwaves and wildfires over the Southwestern United States, devastating floods over Australia, Bangladesh, China and Venezuela, and deadly hurricanes over the North Atlantic[3–5].

Multiyear La Niñas have remarkably more enduring impacts than single-year La Niñas because their persistence creates substantially vaster sea surface temperature (SST) anomalies in the Pacific and Indian oceans (Fig. 1b,c). Multiyear La Niñas induce lasting wet anomalies

[1]Department of Atmospheric Sciences and International Pacific Research Center, School of Ocean Earth Science and Technology, University of Hawaii, Honolulu, HI, USA. [2]Key Laboratory of Virtual Geographic Environment (Ministry of Education) and State Key Laboratory Cultivation Base of Geographical Environment Evolution, School of Geography, Nanjing Normal University, Nanjing, China. [3]Jiangsu Center for Collaborative Innovation in Geographical Information Resource Development and Application, Nanjing, China. [4]Xinjiang Key Laboratory of Oasis Ecology, College of Geography and Remote Sensing Science, Xinjiang University, Urumqi, China. [5]Water Resources Research Center, University of Hawaiʻi at Mānoa, Honolulu, HI, USA. [6]Key Laboratory of Meteorological Disaster (Ministry of Education) and Earth System Modeling Center, Nanjing University of Information Science and Technology, Nanjing, China. [7]NOAA/Geophysical Fluid Dynamics Laboratory, Princeton, NJ, USA. [8]University Corporation for Atmospheric Research, Boulder, CO, USA. [9]NOAA/Pacific Marine Environment Laboratory, Seattle, WA, USA. [10]Lamont-Doherty Earth Observatory, Columbia University, Palisades, NY, USA. [11]School of Atmospheric Sciences, Key Laboratory of Tropical Atmosphere-Ocean System (Ministry of Education) and Southern Marine Science and Engineering Guangdong Laboratory, Sun Yat-sen University, Zhuhai, China. ✉e-mail: wangbin@hawaii.edu; weiyisun@njnu.edu.cn
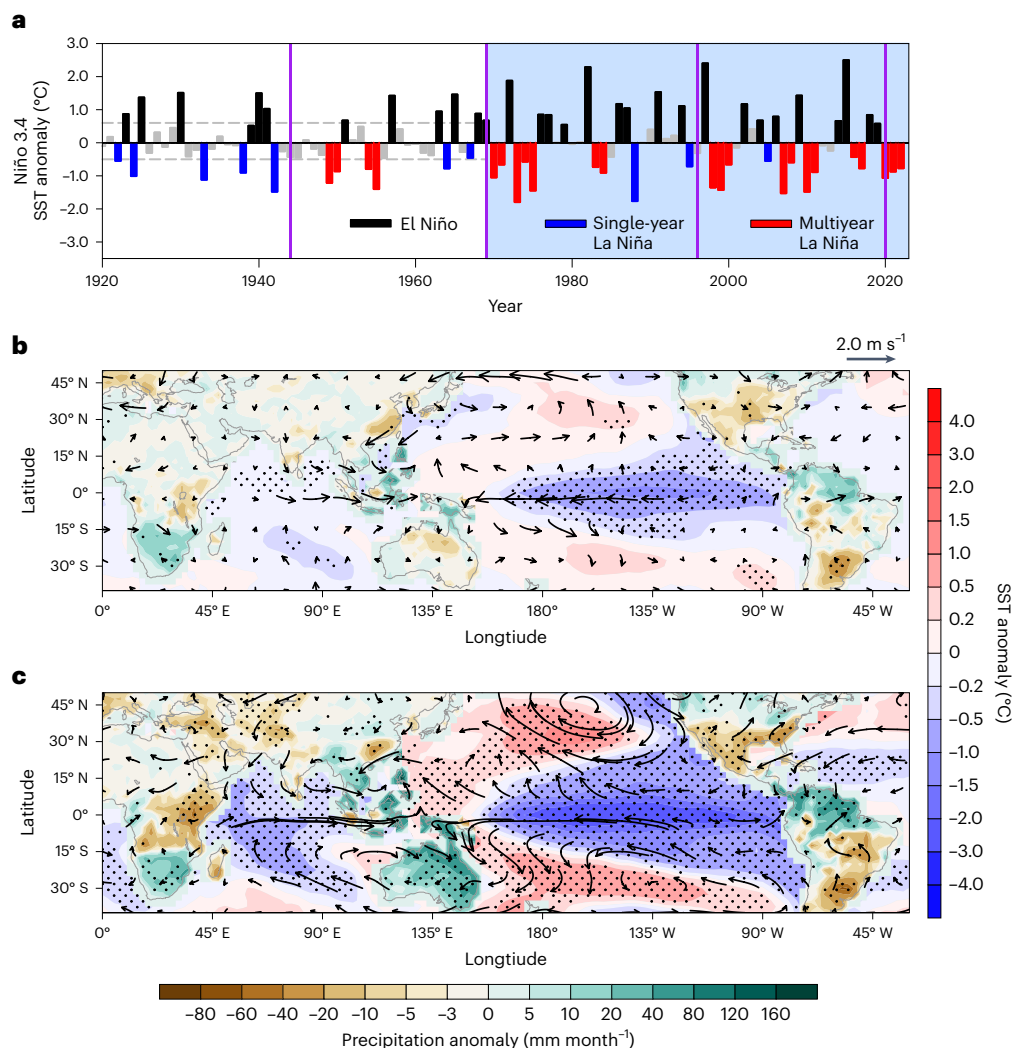
Fig. 1 | Historical change of La Niña (1921–2022). a, Temporal evolution of the Niño 3.4 SST anomaly. A La Niña year is defined by the below-normal (<−0.5 °C) Niño 3.4 Index, the SST anomaly averaged over the index region (5° S–5° N, 120–170° W), during its mature phase from ONDJF. A multiyear La Niña lasts at least two consecutive La Niña years. The grey bars represent neutral years. Blue shading indicates the period of 1970–2022. **b,c**, Comparisons of the composite accumulative climate anomalies averaged for ten single-year La Niña events (**b**) and ten multiyear La Niña events (**c**) during the period of 1920–2022. The accumulative anomalies are the sum of the ONDJF mean anomalies during each year of the entire event, including the land precipitation (mm month^{-1}), SST (°C) and 850 hPa wind (m s^{-1}) anomalies. The stippled areas denote a significance level of 0.05 by a two-tailed Student's t-test. Data used are described in Methods.

over Australia, Indonesia, tropical South America and southern Africa as well as dry anomalies over the Southern United States, Equatorial Africa, India and southeast China. A multiyear La Niña may also prompt a more robust than normal and longer-lasting land response to the land–atmosphere coupling. On the other hand, SST anomalies induced by single-year La Niñas are confined to the equatorial central Pacific (CP) and the precipitation anomalies are weak. Indeed, the single-year events are without significant precipitation anomalies over Australia, India, Africa, North America and Brazil. Even the first-year-only anomalies of the multiyear La Niña show stronger SST anomalies and more significant impacts on precipitation over Australia, Africa and South America (Extended Data Fig. 1).

A prevailing hypothesis for strong or multiyear La Niñas suggests that such events are primarily caused by the preceding extreme El Niño and attendant massive upper ocean heat content discharge that takes many years to recover[6–8]. This perception explains La Niña episodes after three super El Niño (SE) events (1982–1983, 1997–1998 and 2015–2016), albeit the 2016 La Niña was marginal. However, three recent multiyear La Niña episodes (2007–2008, 2010–2011 and 2020–2022) did not follow a super or strong El Niño (Fig. 1a), suggesting the existence

of an alternative route to multiyear La Niñas. Furthermore, La Niña's persistence has been ascribed to diverse sources, including intensive ocean discharge by a strong preceding El Niño[6,7], anomalous Ekman heat transport in the decay period weakening the recharge process[8], nonlinearity in the delayed thermocline feedback[9], thermodynamic processes[10] and the influences from mid-latitude[11] or interbasin interaction[5,12,13]. The critical factors determining the frequency, duration and intensity change of multiyear La Niñas continue to be elusive.

Whether multiyear La Niñas will become more common is an urgent societal concern. Although it is well recognized that global warming affects La Niña properties by changing mean background states[14–17], climate models' projections of La Niña remain inconclusive[18–20], partly due to their mean state biases in the current climate and ENSO nonlinearity[21,22]. Additionally, the reasons for future change of multiyear La Niñas remain obscure. Given the models' caveats, we first investigate how the observed extreme La Niña events have changed with mean state variations over the past century and then examine the Community Earth System Model Version 2 (CESM2) climate models' large ensemble simulation results, hoping to better understand the mechanism of multiyear La Niñas and anticipate future changes.

Historical changes in La Niña properties

There were 20 La Niña events from 1921 to 2022, including ten single-year and ten multiyear events, totalling 33 La Niña years. Notably, multiyear La Niñas have an evident accelerating trend (Fig. 1a). All five events in the first 25 years (1921–1945) are single-year La Niñas, but five out of six in the last 25 years (1998–2022) are multiyear La Niñas. Regarding La Niña years, the historical change is statistically significant at a level of $P = 0.01$ (Supplementary Table 1).

La Niña's intensity has also significantly changed. La Niña and El Niño are highly asymmetric in amplitude, duration and transition[23,24]. Since La Niña usually has weaker intensity than El Niño but lasts longer, using a single-year intensity to measure La Niña severity is inadequate. We propose quantifying La Niña severity by accumulative intensity, a combined measure of yearly intensity and lifespan. The accumulative intensity is defined by the sum of the mean Niño 3.4 Index during each year of the entire La Niña event from October to the following February (ONDJF). For instance, the accumulative intensity of the 1998–2000 La Niña (−3.45 °C) is the sum of the ONDJF Niño 3.4 Index in 1998 (−1.34 °C), 1999 (−1.43 °C) and 2000 (−0.68 °C). The results suggest that the accumulative intensity is an appropriate and practical measure of the severity of La Niña events (Fig. 1b,c). The average accumulative intensity in the past century is −1.6 °C. The top four events with an accumulative intensity below −2.3 °C, including 1973–1975 (−3.9 °C), 1998–2000 (−3.5 °C), 2010–2011 (−2.4 °C) and 2020–2022 (−2.8 °C), may be considered extreme La Niñas. The 2010–2011 La Niña affected four million Colombians, caused approximately US$7.8 billion of economic losses[25], triggered a persistent 2011–2014 drought in California[26] and the Horn of Africa[27], and continued flooding in Australia[5]. The four extreme La Niña events generally induced similar precipitation anomalies in boreal winter. However, the 2010–2011 event had a weaker influence in Africa due to feeble Indian Ocean cooling and associated weak circulation anomalies, and the 2020–2022 event had notably different impacts over the Southern Hemisphere (Extended Data Fig. 2). The average accumulative intensity has significantly ($P < 0.01$) increased by 71% from −1.17 °C during 1920–1969 (nine events) to −2.0 °C during 1970–2022 (ten events). The increased accumulative intensity is mainly due to the enduring persistence, not the yearly magnitude, because the average yearly intensity was about the same (−1.0 °C) in the two 50-year periods.

Two types of multiyear La Niña involve different processes

The eight multiyear La Niña events since 1970 can be categorized into two types based on their antecedent conditions (Fig. 1a). The first type follows the SE events of 1982, 1997 and 2015, and is called super El Niño-to-multiyear La Niña (SE2ML) (Fig. 2a). The second type, consisting of five events (1970–1971, 1973–1975, 2007–2008, 2010–2011 and 2020–2022), is primarily preceded by a CP-related El Niño (CPE) (Fig. 2b) and is called CPE2ML. The traditional definition of a CP El Niño is based on a snapshot of the maximum SST anomaly location at its peak phase. Our definition of a CP El Niño is based on the El Niño evolution from pre-onset to the peak phase. Thus, a CP El Niño is characterized by (1) the warming and associated westerly anomalies originating from the equatorial western Pacific (WP); (2) the warming propagating (extending) eastward during the development stage; and (3) significant warming in the CP during the mature phase. The 1969, 1972, 2006, 2009 and 2018–2019 warm events meet these criteria (Extended Data Fig. 3).

Composite evolutions of the two types of multiyear event, from the preceding El Niño year (−1) to La Niña onset year (0) and La Niña persistence year (+1), are shown in Fig. 2. The evolutions of each multiyear event suggest the composite evolutions represent individual events reasonably well (Extended Data Fig. 3). SE2ML cooling originates from the CP around June (0), reaching −0.75 °C in September (0) (Fig. 2a) and features a weak first-year La Niña in the CP. In contrast, the CPE2ML cooling starts from the far eastern Pacific around

March (0), rapidly reaching −0.75 °C in June (0), and features a strong, westward-propagating first-year La Niña followed by a decaying second-year La Niña. If we classify the strong 1973–1975 event to the SE2ML, the composite pictures are modified slightly and the above description remains valid.

The two types of multiyear La Niña and single-year La Niña involve different atmosphere–ocean feedback processes. We compare them over the core region of La Niña in the equatorial CP (5° S–5° N, 120° W–180°) (Fig. 3). More detailed longitudinal variations of each process along the Equator are shown in Extended Data Fig. 4. First, we note that the onset of a multiyear La Niña features a substantially stronger cooling tendency than a single-year La Niña. This fact explains why the first-year climate anomalies associated with multiyear La Niña events are significantly greater than single-year events (Extended Data Fig. 1). Thus, the magnitude of the La Niña onset rate or the transition rate from the antecedent El Niño to La Niña distinguishes the ensuing persistence. This fundamental difference can be used as a predictor to anticipate the occurrence of a multiyear or a single-year La Niña.

The onset and persistence of SE2ML are primarily attributed to the thermocline feedback (Fig. 3a). The heat loss associated with the meridional heat advection also plays a significant role in persistence, confirming the role of the intense heat content discharge process[28]. Unlike SE2ML, the onset and persistence of CPE2ML in the CP are mainly due to the zonal advective feedback (Fig. 3b). The thermocline feedback contributes to its persistence. The upwelling feedback contributes to the initiation of cooling in the eastern Pacific (Extended Data Fig. 5). The meridional heat advection generally lags behind the mixed-layer temperature (MLT) tendency (and the zonal advective and thermocline feedbacks) by about a season. Its effect also tends to be offset by the surface heat flux effects. The upwelling feedback has little effect in the CP. Therefore, the onset and persistence in the CP are primarily attributed to the sum of the thermocline and zonal advective feedbacks, with more prominent thermocline feedback in SE2ML and more prominent zonal advective feedback in CPE2ML. However, the upwelling feedback plays a critical role in initiating the CPE2ML that originates from the far eastern Pacific.

Causes of the increasing multiyear La Niña

Pacific mean state changes, whether due to external forcing or internal variability, can modulate El Niño and La Niña. Over the past century, the equatorial WP (5° S–5° N, 130–170° E) has experienced significant warming compared with the equatorial CP (5° S–5° N, 150–170° W) (Extended Data Fig. 6). The zonal SST gradient, measured by SST in the WP minus that in the CP, was 1.37 °C during 1921–1940 and 1.66 °C during 2001–2020, an increase of about 21.2%. Accordingly, the associated easterlies have increased near the dateline (150° E–150° W)[29] and the thermocline depth has shallowed by about 24 m, from 142 m to 118 m.

The WP warming-increased SST gradients can strengthen the zonal advective feedback by increasing mean SST gradients. The WP warming-strengthened easterlies can lift the thermocline and increase upwelling, boosting thermocline and upwelling feedbacks. However, thermocline feedback may be compensated by the thermocline depth variations in response to wind changes[22,30]. The WP warming-strengthened easterlies can enhance the upwelling and poleward currents, promoting meridional heat advection. These coupling processes may alter the occurrence of multiyear La Niñas by changing the onset of the antecedent El Niño and the onset and persistence of La Niña, because these phases are open to background-state modulation, as elaborated below.

First, WP warming may promote a multiyear La Niña by initiating more frequent antecedent SE and CPE events. Both the SE and CPE events initiate in the WP at the beginning of year −1 (Fig. 2). WP warming can shift El Niño onset from the eastern to western Pacific by strengthening zonal advective feedback, leading to more frequent CPE and SE events[29]. This assertion is supported by Fig. 4a: when
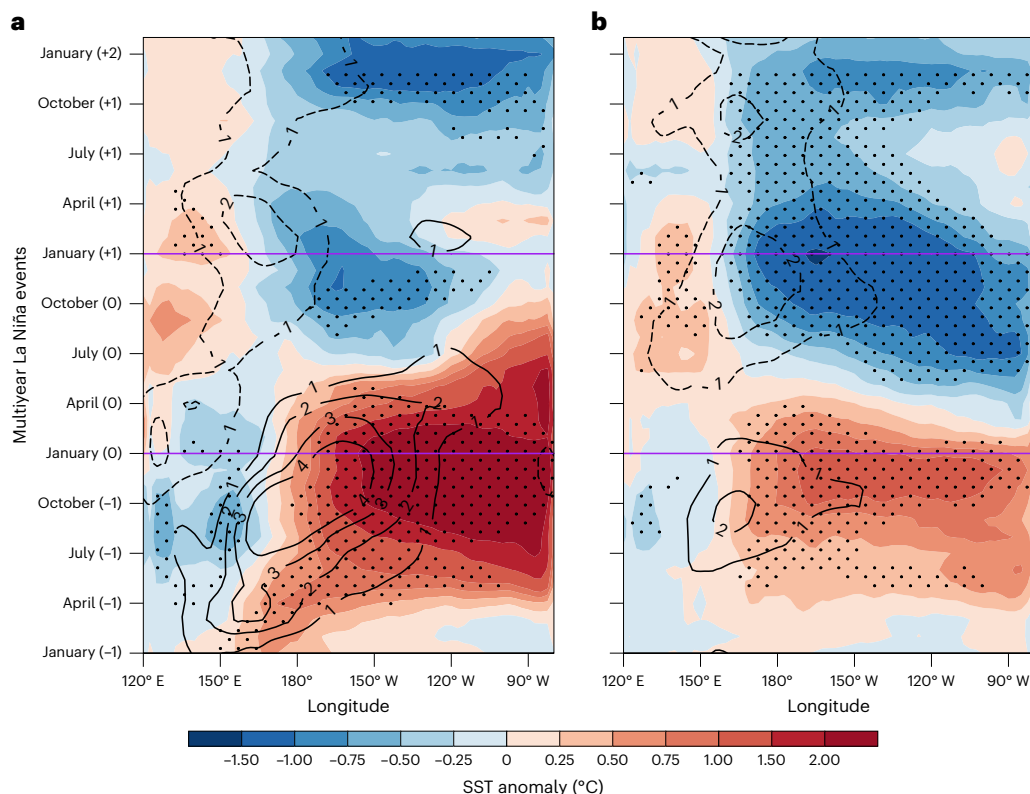
Fig. 2 | Composite evolutions of two types of multiyear La Niña events during the post-1970 period. a,b, Three SE2ML events (1983–1984, 1998–2000, 2016–2017) (**a**) and five CPE2ML events (1970–1971, 1973–1975, 2007–2008, 2010–2011, 2020–2022) (**b**) showing SST (shading, °C) and 1,000 hPa zonal wind (contours, m s⁻¹) anomalies. The stippled areas in SST denote a significance level

of 0.05 by a two-tailed Student's t-test. Horizontal purple lines indicate January (0) and January (1). There were only two double La Niña events before 1970, which followed a neutral ENSO state (Fig. 1a), differing from the eight multiyear La Niña events after 1970.

the WP background SST increases, the antecedent El Niño's warming occurs preferentially in the west-central Pacific (W-CP, 5° S–5° N, 120° E–170° W) with $r = 0.90$ ($P < 0.01$). More frequent CPE and SE events would increase the odds for CPE2ML and SE2ML events. This also means that extreme El Niño and La Niña events may share a common origin in WP warming.

Second, the WP warming-enhanced zonal advective and thermocline feedbacks favour the recent rapid transition of CPE events to multiyear La Niñas (Fig. 3b). We find that the La Niña onset rate is, to a large degree, an indication of its accumulative intensity or persistence (Fig. 4b). Here the 'La Niña onset' rate is measured by the cold tongue (5° S–5° N, 180–90° W) SST anomaly tendency from March (0) to October (0) of the first-year La Niña. A faster onset corresponds to a higher accumulative intensity with a significant positive correlation ($r = 0.64$, $P < 0.01$) for all 20 La Niña events (Fig. 4b). Physically, a fast onset means a sizeable discharge of heat content at its mature phase that takes longer to recover. This assertion is supported by a significant positive correlation between the onset rate and the accumulative thermocline depth anomaly from April (0) to March (+1) (Fig. 4c), indicating more upper ocean heat discharge in the La Niña mature phase. The La Niña onset rate provides a predictor for La Niña's accumulative intensity. It also helps to foretell if a CPE will lead to a multiyear La Niña.

The observed results in Fig. 4a,b are further verified by examining the CESM2 Large Ensemble experiments that participated in Coupled Model Intercomparison Project Phase 6 (CMIP6) historical runs (Methods). The CESM2 can reasonably reproduce the observed ENSO[31]. The ten CESM2 ensemble simulations included 288 La Niña events from 1901 to 2013. The models' WP warming increases the frequencies of the antecedent El Niño that originated from the west Pacific (SE and CPE)

with $r = 0.48$ ($P < 0.01$) (Fig. 4d). The faster-growing La Niña events tend to lead to a larger accumulative intensity ($r = 0.64$, $P < 0.01$) (Fig. 4e). Furthermore, the 30-year mean WP SST increased from the 1901–1930 period to the 1981–2010 period by a mean value of 0.24 °C (Extended Data Fig. 7). During 1901–1930, the number of single-year events (56) is comparable to the number of multiyear events (52). However, during 1981–2010, the number of multiyear events (91) is nearly three times that of single events (32). This change is statistically significant ($P < 0.01$) (Supplementary Table 2). We illustrate the total number of multiyear La Niña years that occurred during 1901–1930 and 1991–2010 as a function of the corresponding 30-year mean WP SST (Fig. 4f). The number of multiyear La Niña years increases with rising WP SST with a significant correlation of 0.52 ($P < 0.05$).

Discussion

This study shows an accelerated trend of multiyear La Niñas over the past century (Fig. 1). There were only two multiyear La Niña events before 1970, and these followed a neutral ENSO state (Fig. 1a), differing from the eight multiyear La Niña events after 1970 that followed an El Niño. The eight multiyear events after 1970 form two types of multiyear La Niña, which are categorized as SE2ML and CPE2ML (Fig. 2). The CPE2ML is an emerging form of multiyear La Niña in recent decades. We postulate that both types arise from WP warming (or increased SST gradients in the west-to-central Pacific) that enhanced atmosphere–ocean coupling. The La Niña onset rate is found to foretell its accumulative intensity and severity of its climate impacts, providing a precursor for predicting extreme La Niñas. The WP warming-enhanced zonal advective and thermocline feedback processes are responsible for the rapid onset and persistence of multiyear La Niñas, distinguishing them from single-year La Niñas (Fig. 3).
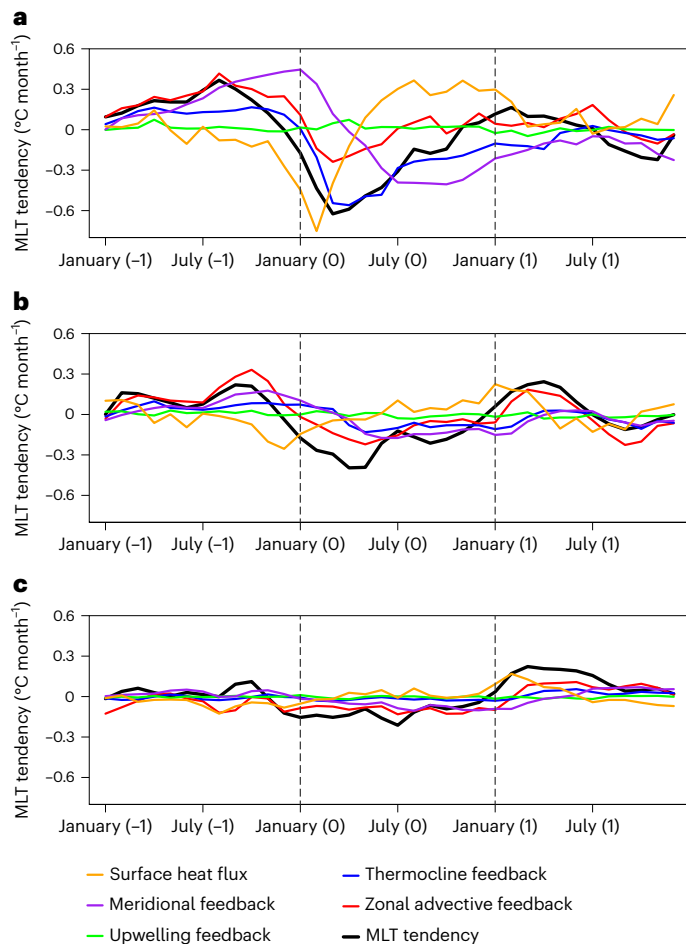
Fig. 3 | Oceanic mixed-layer temperature tendency analyses. a–c, Analyses of SE2ML (**a**), CPE2ML (**b**) and single-year La Niñas (**c**) over the equatorial CP (5° S–5° N, 180°–120° W) covering the preceding El Niño year (−1), La Niña onset year (0) and La Niña persistence year (1). The MLT tendency (°C month⁻¹, black) is mainly attributed to five processes: zonal heat advection by anomalous currents (zonal advective feedback, red), vertical heat advection by the mean upwelling (thermocline feedback, blue), vertical heat advection by anomalous upwelling (upwelling feedback, green), meridional heat advection by the mean currents (meridional feedback, purple) and surface heat fluxes (yellow). Vertical dashed lines indicate January (0) and January (1). The linearly detrended anomalies and the climatology during 1920–2022 were used.

The enhanced zonal advective and thermocline feedback processes favour (1) initiating SE and CPE events in the west Pacific (Figs. 2b and 4a), increasing the odds for the occurrence of multiyear La Niñas; and (2) promoting the fast transition of SE and CPE events to La Niña (Fig. 3b), leading to a sizeable cooling rate and heat discharge. Many of the observed features of multiyear La Niñas find support from the CESM2 Large Ensemble experiments during historical simulation (1901–2013), lending confidence to the conclusions obtained from the limited number of observed La Niña events (Fig. 4d–f).

These findings shed light on the factors that may promote escalating extreme La Niñas in a future warming world. The perception moves beyond the notion that links extreme El Niño and La Niña events to eastern Pacific warming and attributes the changes in these occurrences to different sources. The WP relative warming may affect both extreme El Niño and La Niña events by shifting El Niño onset from the eastern to western Pacific[29] and favouring a fast transition to a persistent La Niña. The knowledge gained from the historical observations adds a metric to validate the models' fidelity. It provides emergent constraints to reduce the uncertainties in projecting future changes of extreme La Niñas.

One may wonder what distinguishes a double or triple La Niña. The results in Extended Data Fig. 8 indicate that double and triple La Niña events display a similar evolution during the first two years. However, the triple La Niña has a greater onset rate and exhibits stronger cooling in the central-eastern Pacific and stronger easterly anomalies over the WP towards the end of the second year, signifying the persistence into the third year. The mixed-layer heat budget results show that during the onset year (0), the double and triple La Niña events are dominated by similar physical processes (Extended Data Fig. 9). However, during the first persistence year (1), the zonal advective and thermocline feedbacks are stronger in the triple La Niña events, leading to the second persistence year of La Niña.

Preliminary analysis of CMIP6 models indicates that most models cannot reproduce the observed moderate SE and CPE events originating from the west Pacific. Many CMIP6 models cannot correctly reproduce ENSO asymmetry, La Niña's persistence or the frequency of multiyear La Niñas, preventing the faithful projection of future change in extreme La Niñas. Current climate models suffer considerable cold tongue bias[18–20], and the projected Pacific mean states are inconsistent across models[32]. Most, though not all, of the latest generation of climate models still cannot reproduce the trends in the observed tropical SST[33], making it difficult to use multiple models to test the observed WP warming impacts on ENSO diversity and multiyear La Niñas. Improving these model defects requires an urgent community effort.

There are ten CPE cases, among which only five are followed by a multiyear La Niña. However, the La Niña onset rate following a CPE can help to anticipate which of these is likely to lead to a multiyear La Niña. As shown in Extended Data Fig. 10, following all ten CPE events, the La Niña onset rate is significantly correlated with its accumulative intensity ($r = 0.65$, $P < 0.05$), implying that a rapid transition from CPE to La Niña is likely to lead to a large accumulative intensity or persistence into a multiyear La Niña due to an intense heat discharge by zonal and thermocline feedbacks (Fig. 4c). Despite this predictor, we need to explore other mechanisms that explain why some El Niño events lead to a multiyear La Niña, while others do not. Fully understanding multiyear La Niña dynamics requires considering many other possibilities, including influences from mid-latitude and the Indian or Atlantic oceans[5,7,11–13], the role of eastern Pacific mean state change, triggering mechanisms arising from the interaction between the annual cycle and high-frequency mode, among others.

The root causes of the Pacific mean state change over the past century remains an open issue. On the one hand, GHG-forced warming in the western tropical Pacific has reached its highest level in the historical record, and further warming in the equatorial Pacific will ensure that record-setting high temperatures will be experienced for decades to come[21,34]. GHG warming could also slow down the Atlantic Meridional Overturning Circulation and warm the tropical South Atlantic, strengthening the Pacific trade winds through interbasin teleconnection[35]. On the other hand, internal variabilities and randomly changing El Niño and La Niña events due to their nonlinear asymmetry could rectify the Pacific mean state[36,37]. Nevertheless, to what extent the relative WP warming is attributed to anthropogenic forcing requires in-depth investigation. However, the potential future intensification of SST difference between the western and central Pacific may play a vital role in the increasing compound impacts of severe El Niño and La Niña events.

Online content

Any methods, additional references, Nature Portfolio reporting summaries, source data, extended data, supplementary information, acknowledgements, peer review information; details of author contributions and competing interests; and statements of data and code availability are available at https://doi.org/10.1038/s41558-023-01801-6.
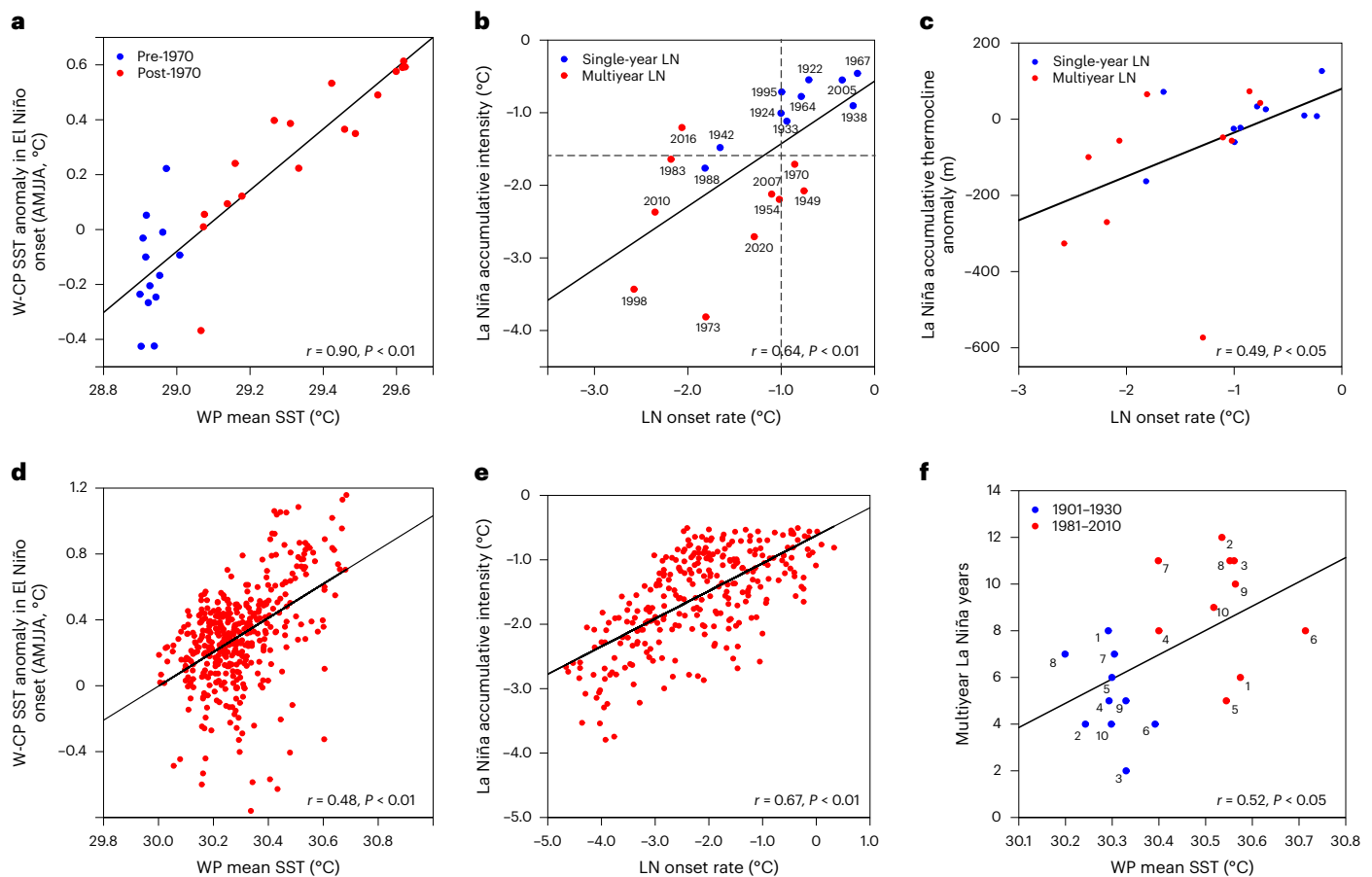
Fig. 4 | Observed and CESM2 model-simulated multiyear La Niña behaviour. **a**, The observed relationship between the antecedent El Niño's initiation in the W-CP and the WP background (31-year running mean) SST. The El Niño initiation is measured by the SST anomaly during the El Niño onset year from April to August (AMJJA). **b**, The observed relationship between the La Niña onset rate and its accumulative intensity. **c**, The observed relationship between the La Niña onset rate and the accumulative thermocline depth anomaly from the cooling onset to March of persistence year (+1). **d**,**e**, CESM2 model-simulated counterparts of **a** (**d**) and **b** (**e**). **f**, The relationship between the 30-year mean WP SST and the number of multiyear La Niña years simulated by ten ensemble members in the CESM2 model's historical simulation (1901–2013). The 30-year means are made for 1901–1930 and 1981–2010 to contrast the significant mean state change.

References

1. Cole, J. E., Overpeck, J. T. & Cook, E. R. Multiyear La Niña events and persistent drought in the contiguous United States. *Geophys. Res. Lett.* **29**, 24–25 (2002).
2. Williams, A. P. et al. Large contribution from anthropogenic warming to an emerging North American megadrought. *Science* **368**, 314–318 (2020).
3. Okumura, Y. M., DiNezio, P. & Deser, C. Evolving impacts of multiyear La Niña events on atmospheric circulation and US drought. *Geophys. Res. Lett.* **44**, 11614–11623 (2017).
4. Cai, W. et al. Increased frequency of extreme La Niña events under greenhouse warming. *Nat. Clim. Change* **5**, 132–137 (2015).
5. Luo, J. J., Liu, G., Hendon, H., Alves, O. & Yamagata, T. Inter-basin sources for two-year predictability of the multi-year La Niña event in 2010–2012. *Sci. Rep.* **7**, 2276 (2017).
6. Iwakiri, T. & Watanabe, M. Mechanisms linking multi-year La Niña with preceding strong El Niño. *Sci. Rep.* **11**, 17465 (2021).
7. Wu, X., Okumura, Y. M. & DiNezio, P. N. What controls the duration of El Niño and La Niña events? *J. Clim.* **32**, 5941–5965 (2019).
8. Iwakiri, T. & Watanabe, M. Contribution of Ekman transport to the ENSO periodicity estimated with an extended Wyrtki index. *Geophys. Res. Lett.* **48**, e2021GL095193 (2021).
9. DiNezio, P. N. & Deser, C. Nonlinear controls on the persistence of La Niña. *J. Clim.* **27**, 7335–7355 (2014).
10. Chen, M., Li, T., Shen, X. & Wu, B. Relative roles of dynamic and thermodynamic processes in causing evolution asymmetry between El Nino and La Nina. *J. Clim.* **29**, 2201–2220 (2016).
11. Park, J. H. et al. Mid-latitude leading double-dip La Niña. *Int. J. Climatol.* **41**, E1353–E1370 (2020).
12. Kim, J. W. & Yu, J. Y. Single- and multi-year ENSO events controlled by pantropical climate interactions. *npj Clim. Atmos. Sci.* **5**, 88 (2022).
13. Hasan, N. A., Chikamoto, Y. & McPhaden, M. J. The influence of tropical basin interactions on the 2020–2022 double-dip La Niña. *Front. Clim.* **4**, 1001174 (2022).
14. Wang, B. Interdecadal changes in El Niño onset in the last four decades. *J. Clim.* **8**, 267–285 (1995).
15. Fedorov, A. V. & Philander, S. G. Is El Niño changing? *Science* **288**, 1997–2002 (2000).
16. DiNezio, P. N., Deser, C., Okumura, Y. & Karspeck, A. Predictability of 2-year La Niña events in a coupled general circulation model. *Clim. Dynam.* **49**, 4237–4261 (2017).
17. Choi, J., An, S. I., Kug, J. S. & Yeh, S. W. The role of mean state on changes in El Niño's flavor. *Clim. Dynam.* **37**, 1205–1215 (2011).
18. Fredriksen, H. B., Berner, J., Subramanian, A. C. & Capotondi, A. How does El Niño–Southern Oscillation change under global warming—a first look at CMIP6. *Geophys. Res. Lett.* **47**, e2020GL090640 (2020).

19. Collins, M. et al. The impact of global warming on the tropical Pacific Ocean and El Niño. *Nat. Geosci.* **3**, 391–397 (2010).

20. Chen, C., Cane, M. A., Wittenberg, A. T. & Chen, D. ENSO in the CMIP5 simulations: life cycles, diversity, and responses to climate change. *J. Clim.* **30**, 775–801 (2017).

21. Seager, R. et al. Strengthening tropical Pacific zonal sea surface temperature gradient consistent with rising greenhouse gases. *Nat. Clim. Change* **9**, 517–522 (2019).

22. Kohyama, T., Hartmann, D. L. & Battisti, D. S. Weakening of nonlinear ENSO under global warming. *Geophys. Res. Lett.* **45**, 8557–8567 (2018).

23. Okumura, Y. M. & Deser, C. Asymmetry in the duration of El Niño and La Niña. *J. Clim.* **23**, 5826–5843 (2010).

24. An, S. I. & Jin, F. F. Nonlinearity and asymmetry of ENSO. *J. Clim.* **17**, 2399–2412 (2004).

25. Hoyos, N., Escobar, J., Restrepo, J. C., Arango, A. M. & Ortiz, J. C. Impact of the 2010–2011 La Niña phenomenon in Colombia, South America: the human toll of an extreme weather event. *Appl. Geogr.* **39**, 16–25 (2013).

26. Seager, R. et al. Causes of the 2011–14 California drought. *J. Clim.* **28**, 6997–7024 (2015).

27. Anderson, W. et al. Multi-year La Niña events and multi-season drought in the Horn of Africa. *J. Hydrometeorol.* **24**, 119–131 (2023).

28. Jin, F. F. An equatorial ocean recharge paradigm for ENSO. Part I: conceptual model. *J. Atmos. Sci.* **54**, 811–829 (1997).

29. Wang, B. et al. Historical change of El Niño properties shed light on future changes of extreme El Niño. *Proc. Natl Acad. Sci. USA* **116**, 22512–22517 (2019).

30. Lubbecke, J. F. & McPhaden, M. J. Assessing the twenty-first-century shift in ENSO variability in terms of the Bjerknes stability index. *J. Clim.* **27**, 2577–2587 (2014).

31. Capotondi, A., Deser, C., Phillips, A. S., Okumura, Y. & Larson, S. M. ENSO and Pacific decadal variability in the Community Earth System Model Version 2. *J. Adv. Model. Earth Syst.* **12**, e2019MS002022 (2022).

32. Xiang, B., Wang, B., Li, J., Zhao, M. & Lee, J. Y. Understanding the anthropogenically forced change of equatorial Pacific trade winds in coupled climate models. *J. Clim.* **27**, 8510–8526 (2014).

33. Seager, R., Henderson, N. & Cane, M. Persistent discrepancies between observed and modeled trends in the tropical Pacific Ocean. *J. Clim.* **35**, 4571–4584 (2022).

34. Power, S. et al. Decadal climate variability in the tropical Pacific: characteristics, causes, predictability, and prospects. *Science* **374**, eaay9165 (2021).

35. Orihuela-Pinto, B., England, M. H. & Taschetto, A. S. Interbasin and interhemispheric impacts of a collapsed Atlantic Overturning Circulation. *Nat. Clim. Change* **12**, 558–565 (2022).

36. Yang, Y. M., An, S. I., Wang, B. & Park, J. H. A global-scale multidecadal variability driven by Atlantic multidecadal oscillation. *Natl Sci. Rev.* **7**, 1190–1197 (2019).

37. McPhaden, M. J., Lee, T. & McClurg, D. El Niño and its relationship to changing background conditions in the tropical Pacific Ocean. *Geophys. Res. Lett.* **38**, L15709 (2011).

Methods

Data used

The SST data used in this work are averages of two monthly mean SST datasets from 1871–2022: (1) the Hadley Centre Sea Ice and SST dataset v.1 (HadISST1) (ref. [38]) and (2) the Extended Reconstructed Sea Surface Temperature Version 5 (ERSSTv5) global SST dataset[39]. The surface winds and atmospheric circulation fields are derived from the European Centre for Medium-Range Weather Forecasts (ECMWF) reanalysis datasets, which are made by merging the ERA-20C reanalysis[40] (1901–1957), ERA 40-year (ERA-40) (ref. [41]) reanalysis (1958–1978) and ERA5 reanalysis[42] (1979–2022). To ensure temporal consistency, we calibrated the mean states of the ERA-40 and ERA5 reanalysis datasets using the data during the overlap period of 1979–2001 and by removing their differences in monthly climatology during the overlap period (1958–2010) from the ERA-20C dataset. The precipitation data are derived from the Global Precipitation Climatology Centre dataset over land from 1901 to 2022[43]. The surface heat flux data are made by merging the NOAA-CIRES 20th Century Reanalysis (1921–2012)[44] and NCEP/DOE Reanalysis II (1979–2022)[45]. We calibrated the mean states of these by removing their differences in monthly climatology during the overlap period. The ocean reanalysis dataset used is primarily from the Simple Ocean Data Assimilation (SODA) v.2.2.4 reanalysis for 1871–2008[46], which is extended from 2009 to 2022 using the Global Ocean Data Assimilation System (GODAS)[47]. The mean state of GODAS is calibrated to SODA based on the overlapping period from 1980 to 2008.

In this work, we used data from the past 100 years (1920–2022), considering the large discrepancy and uncertainty of SST data for the period before 1920 between HadISST and ERSST. We also used linearly detrended data for the analysis. The SST anomaly averaged in the Niño 3.4 region, known as the Niño 3.4 Index, shows maximum variances during ONDJF, with a peak in December[29]. Thus, to select La Niña years, we used ONDJF with mean Niño 3.4 of less than −0.5 °C. There were 20 La Niña events from 1920 to 2022, including ten single-year and ten multiyear La Niñas. The 20 events comprise 33 La Niña years, including 20 onset and 13 consecutive years.

Ocean mixed-layer heat budget

The budget analysis was applied to the composite events for four types of La Niña. To quantify the contributions of different dynamic processes to the El Niño evolution, we used the following ocean MLT tendency equation[15]:

$$\frac{\partial T'}{\partial t} = -(V' \cdot \nabla \bar{T} + \bar{V} \cdot \nabla T' + V' \cdot \nabla T') + R = -\left[\left(\frac{u'\partial\bar{T}}{\partial x} + \frac{\bar{u}\partial T'}{\partial x} + \frac{u'\partial T'}{\partial x}\right)\right.$$
$$\left. + \left(\frac{v'\partial\bar{T}}{\partial y} + \frac{\bar{v}\partial T'}{\partial y} + \frac{v'\partial T'}{\partial y}\right) + \left(\frac{w'\partial\bar{T}}{\partial z} + \frac{\bar{w}\partial T'}{\partial z} + \frac{w'\partial T'}{\partial z}\right)\right] + R,$$

where the overbars and primes denote climatological mean and anomalous quantities, respectively; T is the MLT; $V = (u, v, w)$ refers to the zonal and meridional currents and upwelling velocities, respectively; ρ (= 103 kg m^{-3}) is water density; C_p(= 4,000 J kg K^{-1}) is the specific heat of water; and R is the residual term, including surface heat exchange.

CESM2 Large Ensemble simulations

We used ten historical experiments (1850–2014) obtained from the CESM2 Large Ensemble simulations derived from the latest CESM2 model[48] with CMIP6 historical forcing from 1850 to 2014[49] to support the observed multiyear La Niña behaviour. CESM2, limited by the chemistry, is a 'low-top' version of the atmospheric model and uses the horizontal resolution nominal 1° × 1°. The ocean models are the Parallel Ocean Program v.2 with a uniform spacing of 1.125° in longitude and varying spacing in latitude and provide 60 vertical levels. To ensure the CESM2 model can reproduce reasonably realistic La Niña behaviour, we examined the model's performance on ten simulations using the same method for the observational data to distinguish different types of La Niña simulated by CESM2.

Data availability

All data related to this paper can be downloaded as follows: SST data are derived from the HadISST v.1 (ref. [38]) (https://www.metoffice.gov.uk/hadobs/hadisst/data/download.html) and ERSSTv5 (ref. [39]) (https://psl.noaa.gov/data/gridded/data.noaa.ersst.v5.html); atmospheric circulation fields are derived from ERA-20C reanalysis[40] (https://rda.ucar.edu/datasets/ds626.0/dataaccess), ERA-40 reanalysis[41] (https://www.ecmwf.int/en/forecasts/dataset/ecmwf-reanalysis-40-years) and ERA5 reanalysis[42] (https://www.ecmwf.int/en/forecasts/dataset/ecmwf-reanalysis-v5); precipitation data are available at the Global Precipitation Climatology Centre[43] (https://www.esrl.noaa.gov/psd/data/gridded/data.gpcc.html); surface heat flux data of NCEP reanalysis 2 (ref. [45]) and 20CR v.2 (ref. [44]) are available at https://psl.noaa.gov/data/gridded/data.ncep.reanalysis2.html and https://psl.noaa.gov/data/gridded/data.20thC_ReanV2c.html, respectively; ocean reanalysis data are from SODA v.2.2.4 (ref. [46]) (https://www.atmos.umd.edu/~ocean/index.htm) and GODAS[47] (https://www.esrl.noaa.gov/psd/data/gridded/data.godas.html); CESM2 Large Ensemble simulation[48] outputs are available at https://www.cesm.ucar.edu/community-projects/lens2.

Code availability

Code for the main results is available on Zenodo at https://doi.org/10.5281/zenodo.8196384 (ref. [50]).

References

38. Rayner, N. A. et al. Global analyses of sea surface temperature, sea ice, and night marine air temperature since the late nineteenth century. *J. Geophys. Res. Atmos.* **108**, 4407 (2003).
39. Huang, B. et al. Extended reconstructed sea surface temperature, version 5 (ERSSTv5): upgrades, validations, and intercomparisons. *J. Clim.* **30**, 8179–8205 (2017).
40. Poli, P. et al. ERA-20C: an atmospheric reanalysis of the twentieth century. *J. Clim.* **29**, 4083–4097 (2016).
41. Uppala, S. M. et al. The ERA-40 re-analysis. *Q. J. R. Meteor. Soc.* **131**, 2961–3012 (2005).
42. Hersbach, H. et al. The ERA5 global reanalysis. *Q. J. R. Meteor. Soc.* **146**, 1999–2049 (2020).
43. Schneider, U. et al. GPCC's new land surface precipitation climatology based on quality-controlled in situ data and its role in quantifying the global water cycle. *Theor. Appl. Climatol.* **115**, 15–40 (2014).
44. Compo, G. P. et al. The Twentieth Century Reanalysis project. *Q. J. R. Meteorol. Soc.* **137**, 1–28 (2011).
45. Kanamitsu, M. et al. NCEP-DOE AMIP-II Reanalysis (R-2). *Bull. Am. Meteorol. Soc.* **83**, 1631–1643 (2002).
46. Carton, J. A. & Giese, B. S. A reanalysis of ocean climate using Simple Ocean Data Assimilation (SODA). *Mon. Weather Rev.* **136**, 2999–3017 (2008).
47. Behringer, D. W., Ji, M. & Leetmaa, A. An improved coupled model for ENSO prediction and implications for ocean initialization. Part I: the ocean data assimilation system. *Mon. Weather Rev.* **126**, 1013–1021 (1998).
48. Danabasoglu, G. et al. The Community Earth System Model Version 2 (CESM2). *J. Adv. Model. Earth Syst.* **12**, e2019MS001916 (2020).
49. O'Neill, B. C. et al. The scenario model intercomparison project (ScenarioMIP) for CMIP6. *Geosci. Model Dev.* **9**, 3461–3482 (2016).
50. Sun, W. Code for 'understanding the recent increase in multiyear La Niñas'. *Zenodo* https://doi.org/10.5281/zenodo.8196384 (2023).

Author contributions

Competing interests

Additional information

Extended data is available for this paper at https://doi.org/10.1038/s41558-023-01801-6.

Supplementary information The online version contains supplementary material available at https://doi.org/10.1038/s41558-023-01801-6.

Correspondence and requests for materials should be addressed to Bin Wang or Weiyi Sun.

Peer review information *Nature Climate Change* thanks Sulian Thual and the other, anonymous, reviewer(s) for their contribution to the peer review of this work.

Reprints and permissions information is available at www.nature.com/reprints.
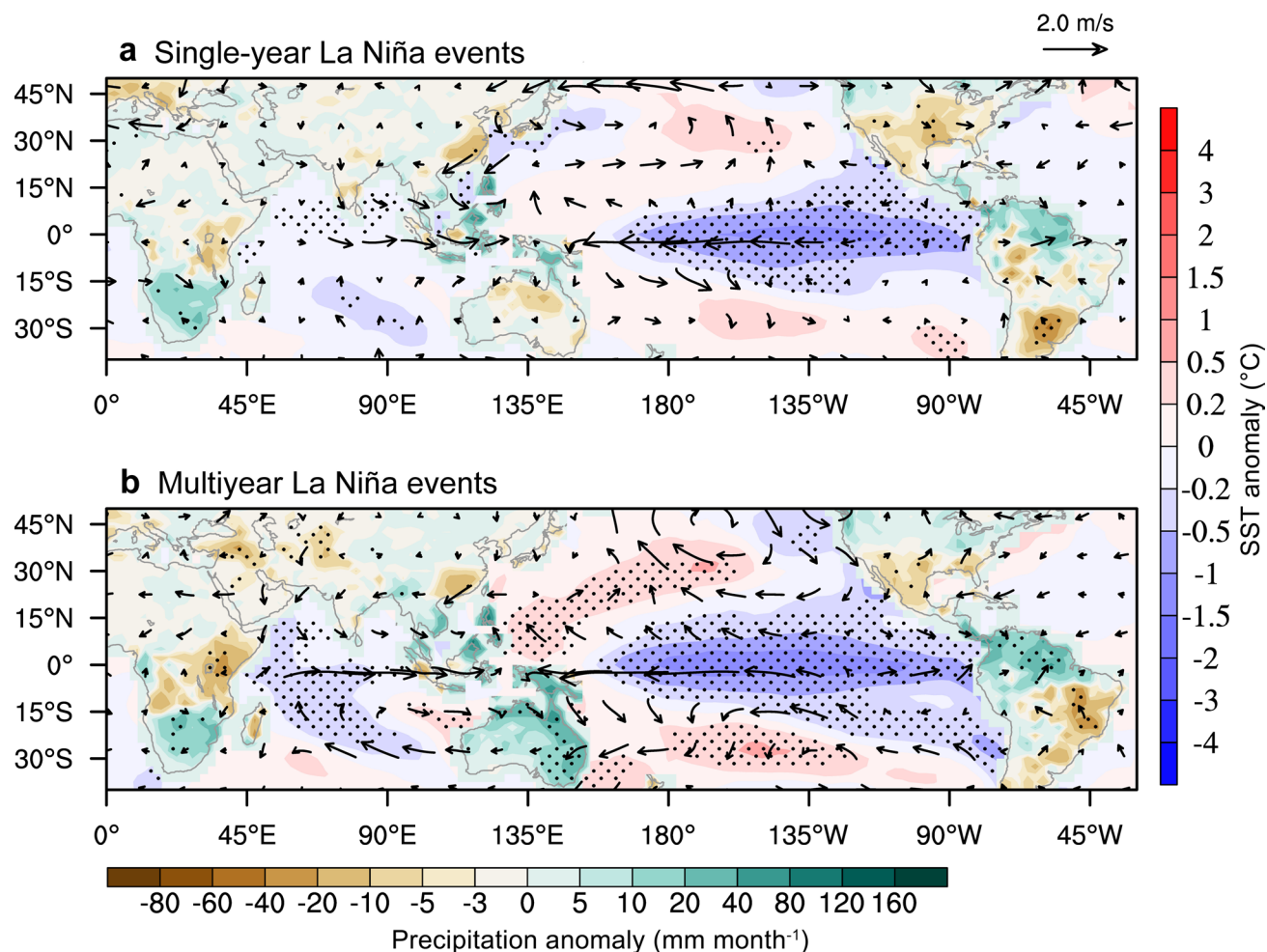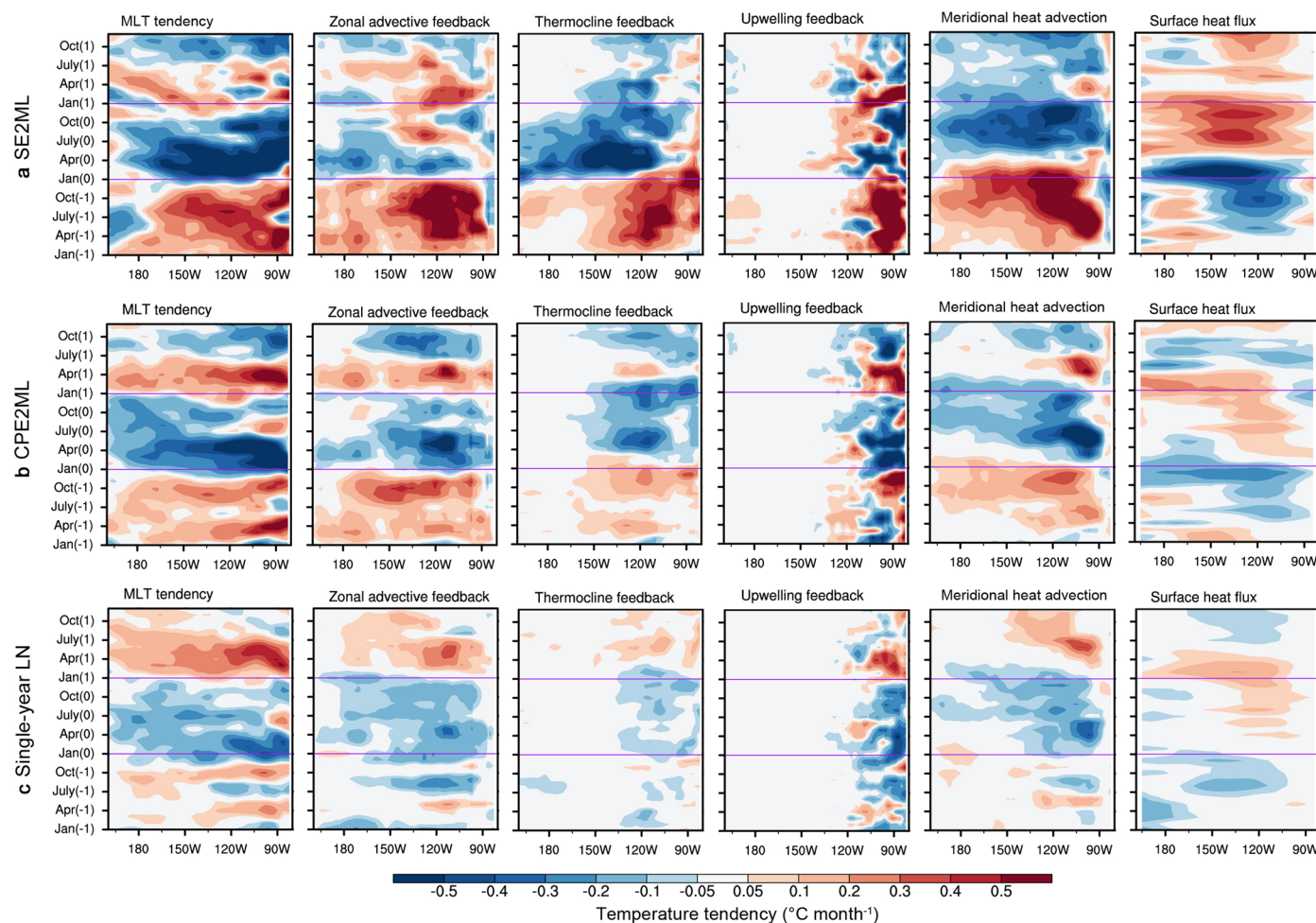
Extended Data Fig. 1 | The first-year climate anomalies associated with single-year and multiyear La Niña events. Shown are the ONDJF land precipitation (mm month⁻¹), SST (°C), and 850 hPa winds (m s⁻¹) averaged for **(a)** ten single-year La Niña events and **(b)** ten multiyear La Niña events during 1920–2022. The stippled areas denote a significant level of 0.05 by a two-tailed Student's t-test. Data used are described in Method.
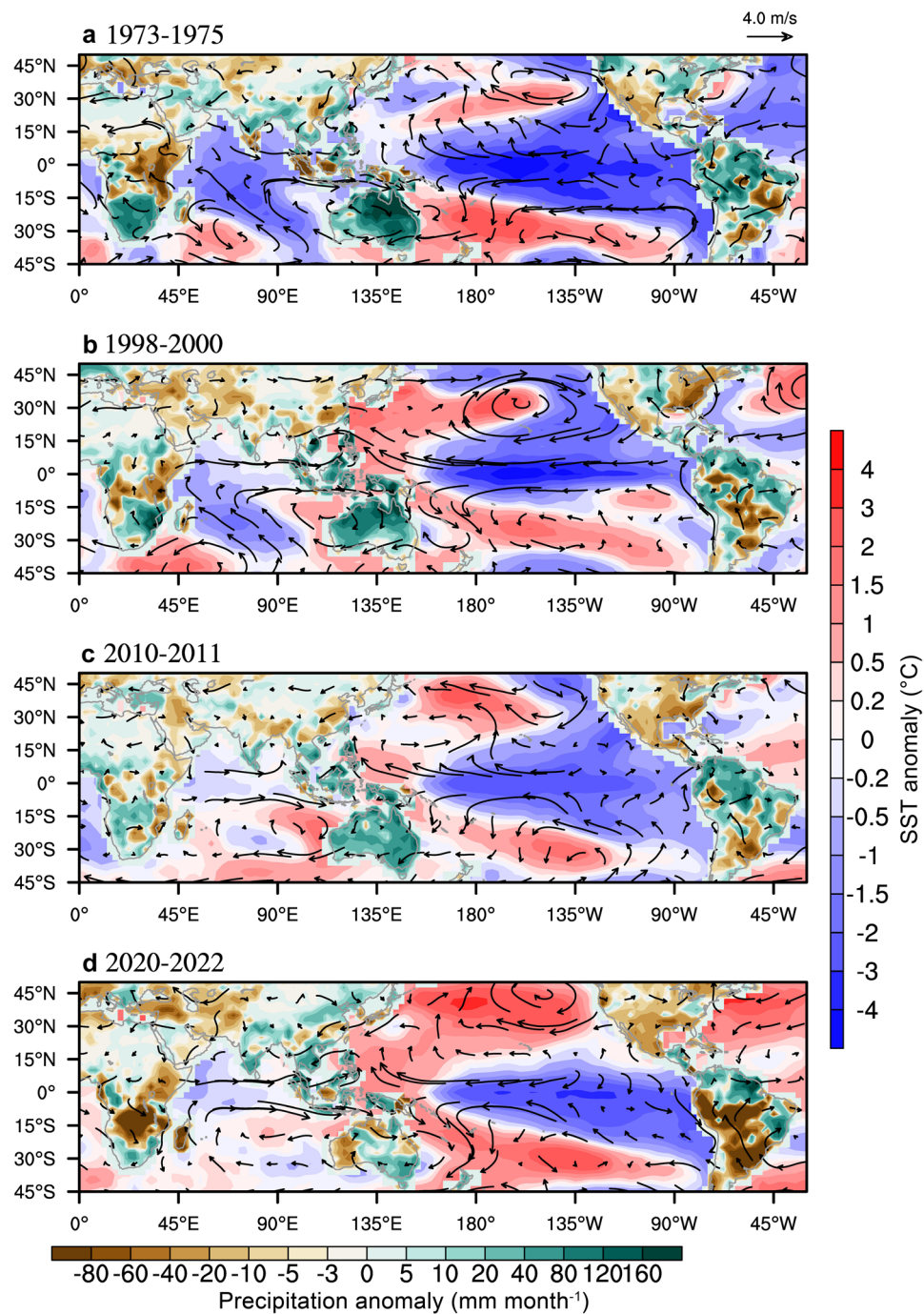
Extended Data Fig. 2 | Climate anomalies associated with four extreme La Niña events. Same as in Fig. 1c except for the extreme La Niña event **(a)** 1973–75, **(b)** 1998–2000, **(c)** 2010–11, and **(d)** 2020–22.

Extended Data Fig. 3 | Evolution of each multiyear La Niña event during the post-1970 period. SST (shading, °C) and 1000hPa zonal wind (contours, m s⁻¹) anomalies.
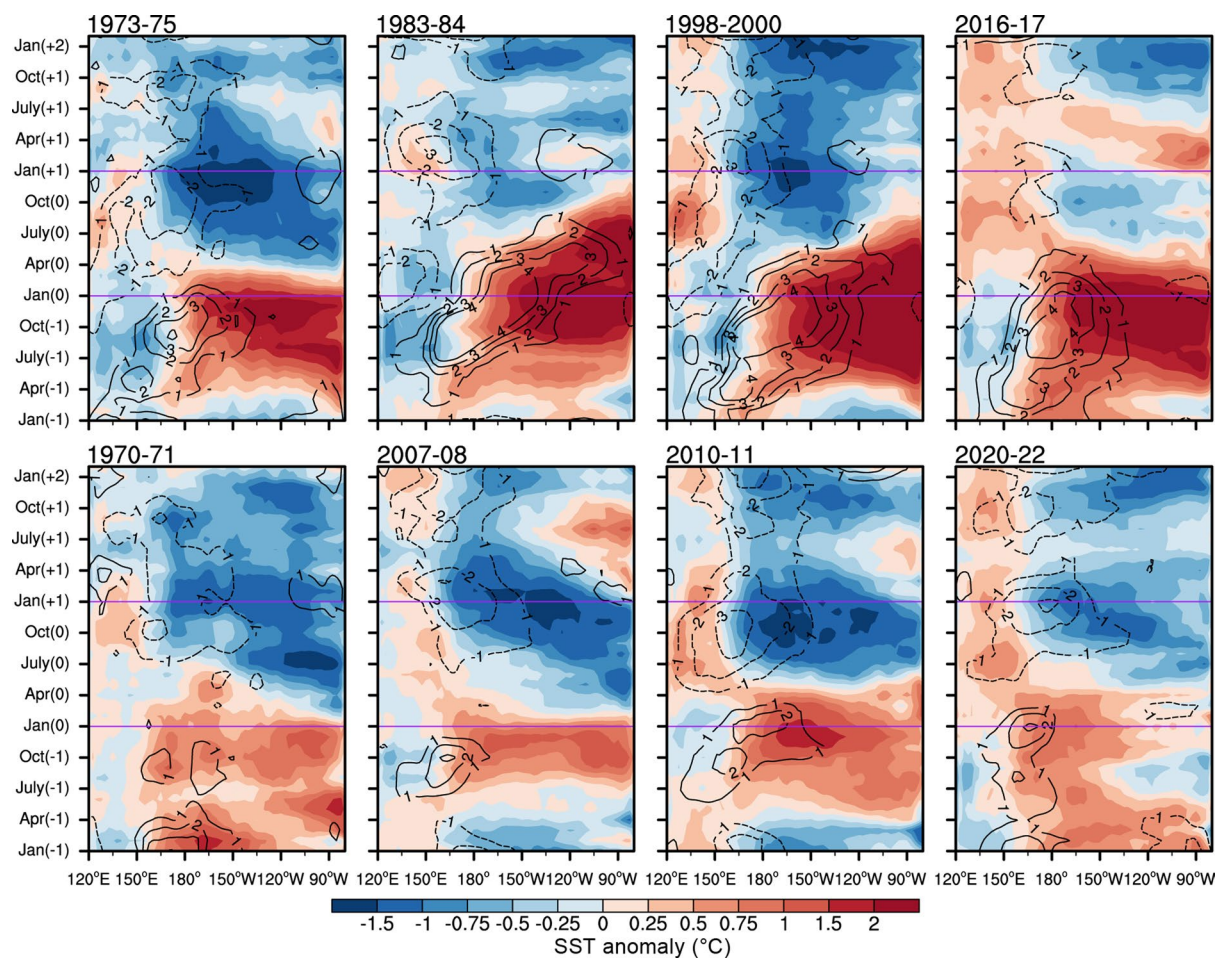
Extended Data Fig. 4 | Oceanic mixed layer temperature tendency analyses. (a) Super-El Niño to multiyear La Niña (SE2ML), (b) central Pacific El Niño to multiyear La Niña (CPE2ML), and (c) single-year La Niña along the equatorial belt. The analysis period (ordinate) covers the antecedent El Niño, Year (−1), La Niña onset, Year (0), and La Niña persistence, Year (1). The processes caused the ML temperature tendency (units: °C month⁻¹) include zonal advective feedback (zonal heat advection by anomalous currents), thermocline feedback (vertical heat advection by the mean upwelling), upwelling feedback (vertical heat advection by anomalous upwelling), meridional heat advection (by the mean currents), and surface heat fluxes. Horizontal purple lines indicate Jan (0) and Jan (1). The linearly detrended anomalies and the climatology during 1920–2022 were used.
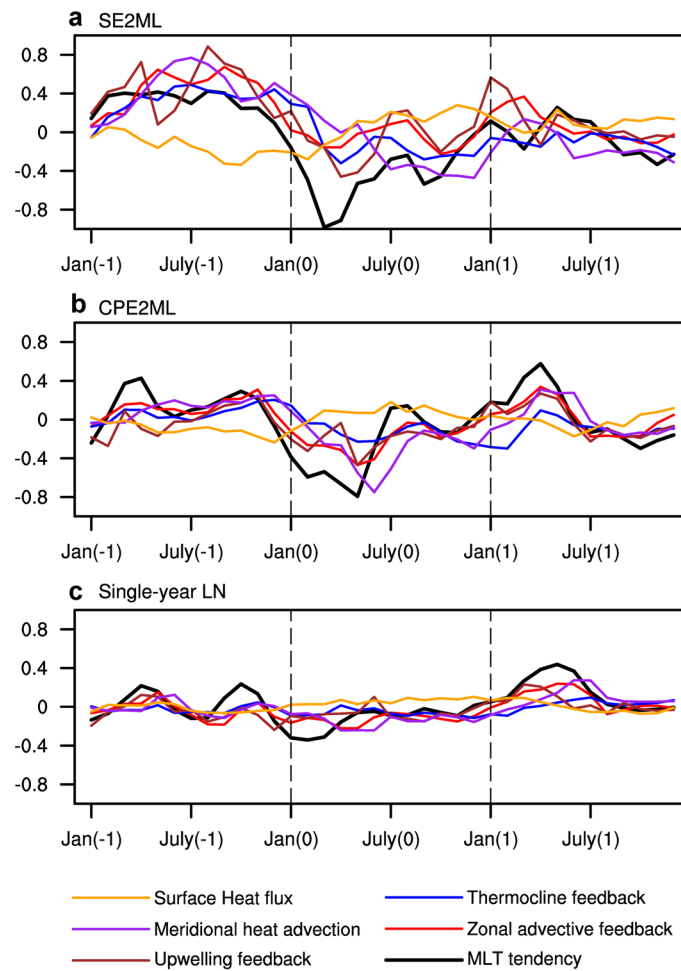
Extended Data Fig. 5 | Oceanic mixed layer temperature tendency analyses of the eastern Pacific. The same as in Fig. 3 except for the eastern Pacific (120°W–80°W). The eastern Pacific bears similar features as the central Pacific, except the upwelling process plays a more prominent role.
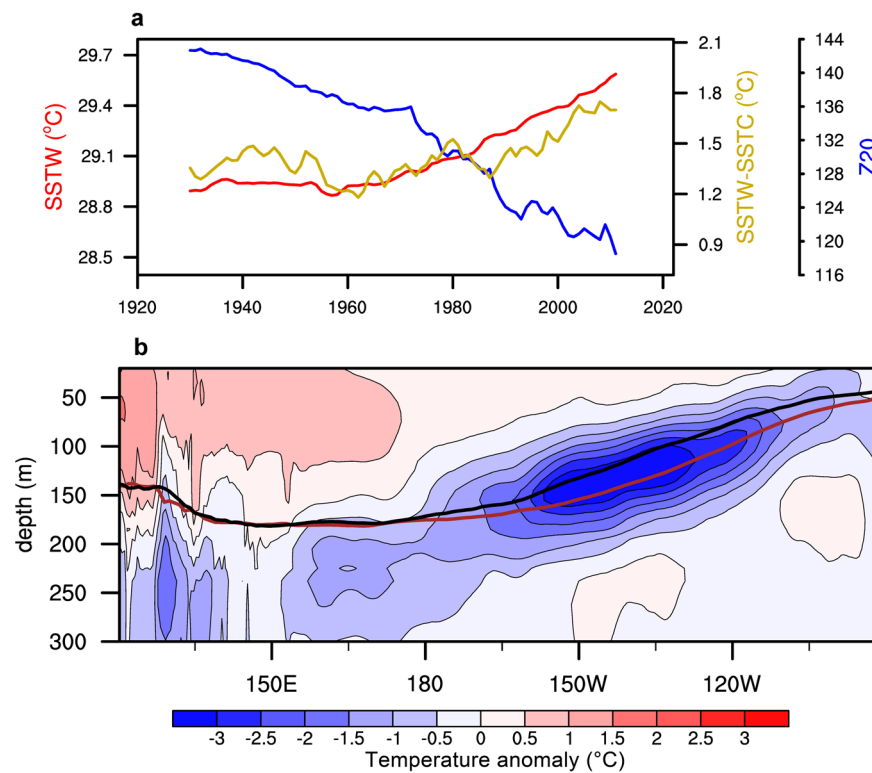
Extended Data Fig. 6 | Mean state change during 1921–2020. (a) 30-year running mean SST over the WP (130°E–170°E, 5°S–5°N) (red line), SSTW minus SSTC (170°W–150°W, 5°S–5°N) (orange line), and thermocline depth (20 °C isotherm, Z20 (m)) averaged in the NINO3.4 region (blue line). **(b)** The change of the equatorial thermocline depth and temperature measured by 20-year mean difference: 2001–2020 minus 1921–1940. Black line represents the thermocline depth during 2001–2020 while brown line represents the thermocline depth during 1921–1940.
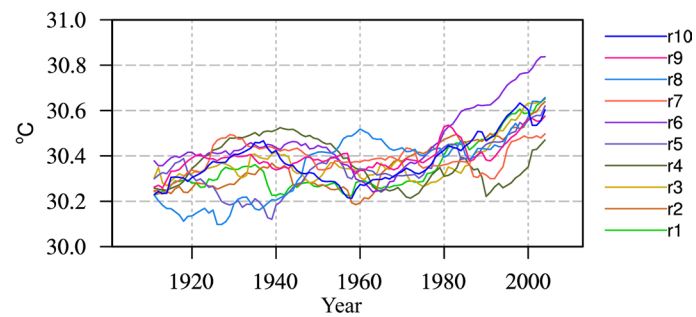
Extended Data Fig. 7 | Simulated western Pacific SST change. The 21-yr running mean SST time series averaged over the WP (130°E–160°E, 5°S–5°N) during 1901–2013 simulated by each of the ten CESM2 ensemble experiments. The warming trends measured by the difference between the last 30-year and the beginning 30-year mean SST vary from 0.10 to 0.35 with a mean of 0.24.
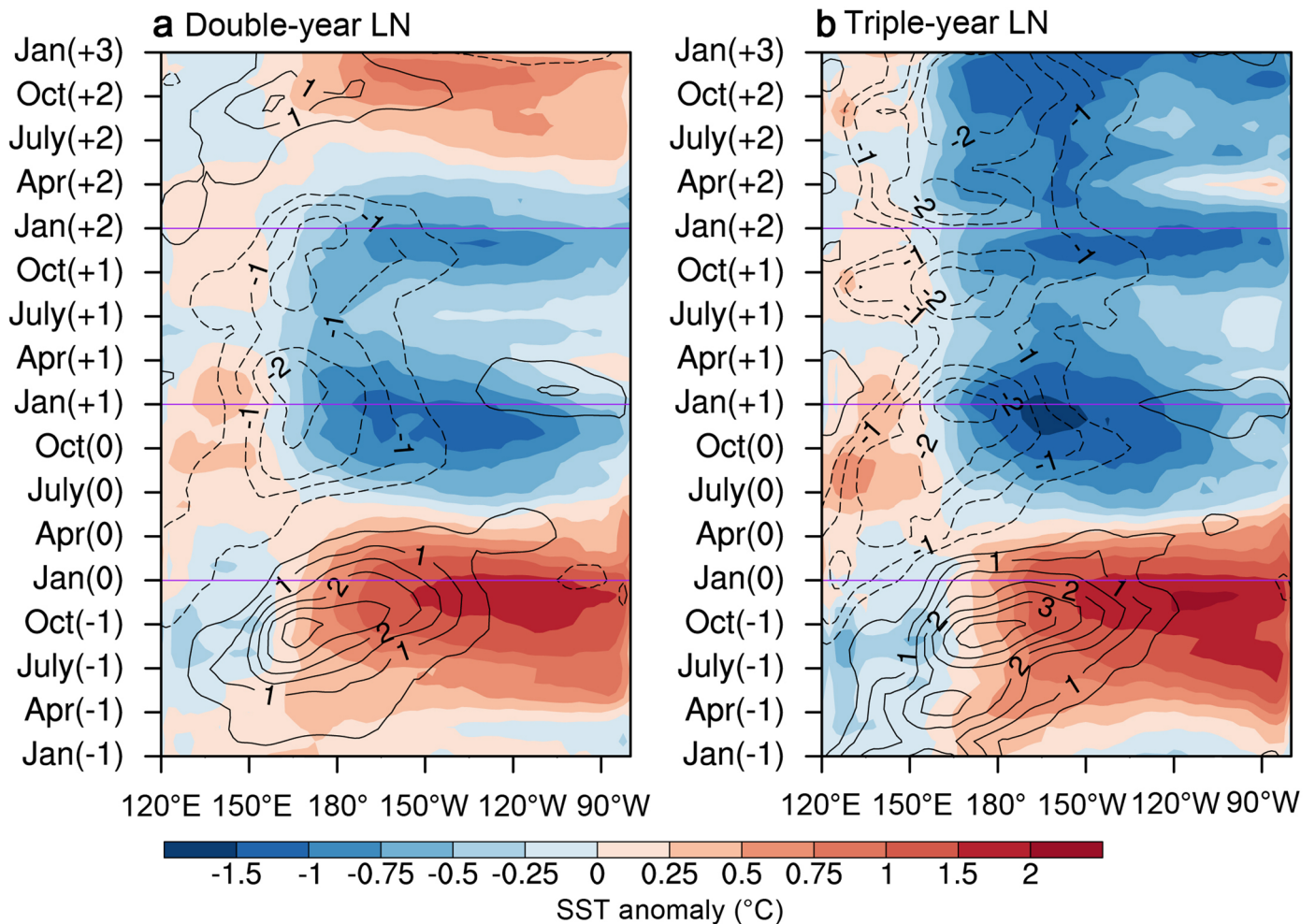
Extended Data Fig. 8 | Composite evolutions of two types of multiyear La Niña events during the post-1970 period. SST (shading, °C) and zonal wind (contours, m s⁻¹) anomalies. (**a**) Five double-year La Niña (1970–71, 1983–84, 2007–08, 2010–11, and 2016–2017), and (**b**) three triple-year La Niña (1973–75, 1998–2000, and 2020–2022). Horizontal purple lines indicate Jan (0) and Jan (1).
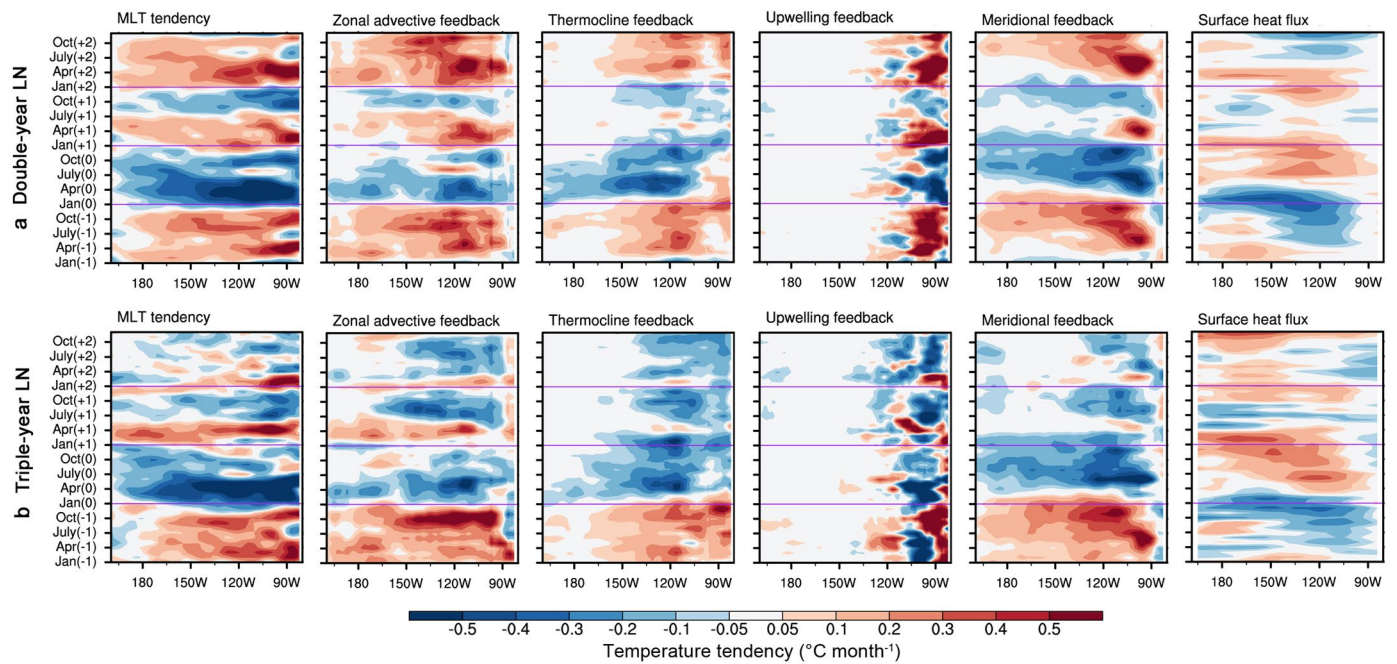
Extended Data Fig. 9 | Oceanic mixed layer temperature tendency analyses. The same as in the Extended Data Fig. 4 except for **(a)** double-year La Niña and **(b)** triple-year La Niña along the equatorial belt.
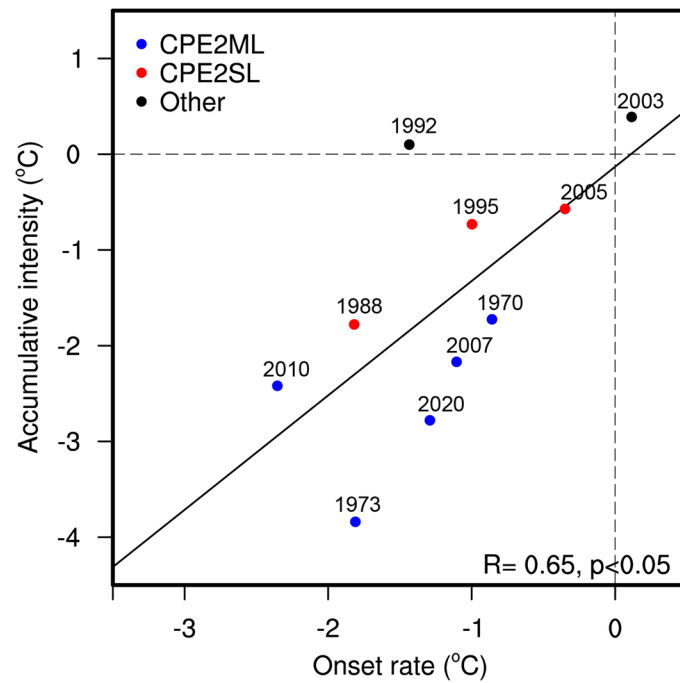
Extended Data Fig. 10 | The observed relationship between the La Niña onset rate following CP El Niño events and its accumulative intensity. The La Niña onset rate following all ten CP El Niño events significantly correlates with its accumulative intensity (r = 0.65, p < 0.05). The onset rate is defined by the NINO 3.4 cooling tendency from March (0) to October (0).